Supplementary Materials
Correlation between Adsorption and Photocatalysis in the Aqueous System Cr(VI)-TiO_2

Jorge M. Meichtry [1,2], Hernán B. Rodríguez [3], María A. Grela [4,†], Enrique San Román [3,†] and Marta I. Litter [5,*]

[1] Centro de Tecnologías Químicas, Facultad Regional Buenos Aires, Universidad Tecnológica Nacional, Medrano 951, Ciudad Autónoma de Buenos Aires 1179, Argentina; jmeichtry@frba.utn.edu.ar (J.M.M.)
[2] Gerencia Química, Comisión Nacional de Energía Atómica and CONICET, Av. Gral. Paz 1499, San Martín 1650, Argentina
[3] Instituto de Química Física de los Materiales, Medio Ambiente y Energía (INQUIMAE, UBA-CONICET), Universidad de Buenos Aires, Ciudad Universitaria, Pabellón 2, Ciudad Autónoma de Buenos Aires 1428, Argentina; hbr@qi.fcen.uba.ar or hernanbrodriguez76@gmail.com (H.B.R.); esr@qi.fcen.uba.ar (E.S.R.)
[4] Departamento de Química, Universidad Nacional de Mar del Plata, Funes 3350, Mar del Plata 7600, Argentina; magrela@mdp.edu.ar (M.A.G.)
[5] IIIA-UNSAM-CONICET, Instituto de Investigación e Ingeniería Ambiental, Escuela de Hábitat y Sostenibilidad (EHyS), Universidad Nacional de San Martín (UNSAM), Campus Miguelete, 25 de mayo y Francia, San Martín 1650, Argentina

* Corresponding author. E-mail: martalitter24@gmail.com or mlitter@unsam.edu.ar (M.I.L.)

† Deceased.

S1. Diffraction Spectrum of The Rutile Sample (UV100 Calcined at 650 °C)

As said in the main text, diffraction (XRD) spectrum of the powdered sample (Figure S1) was obtained at room temperature with a Philips PW-3710 diffractometer using Cu-Kα radiation at a scan rate of 0.02° (2θ/s), an accelerating voltage of 40 kV and an applied current of 30 mA.

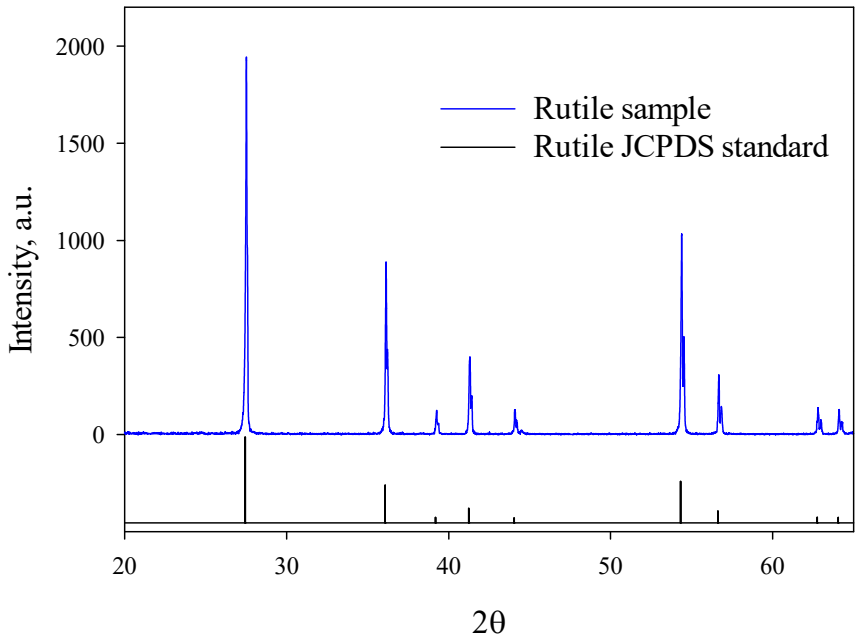

Figure S1. XRD spectrum of the rutile sample. The rutile standard spectrum (ICSD collection code 023697) is added for comparison.

Figure S1 indicates that, after calcination at 650 °C for 2 h, the anatase UV100 sample was 100% transformed into rutile, as confirmed by comparison with the rutile standard spectrum from the ICSD collection (code 023697). The crystal size of the obtained rutile sample can be calculated using the Scherrer equation:

https://doi.org/10.70322/prp.2025.10015

$$D = \frac{0.9\lambda}{\beta \cos\theta} \quad \text{(S1)}$$

where D is the average crystal size, 0.9 is the shape factor, λ is the X-ray wavelength, β is the full width at half maximum of the diffraction peak and θ is the Bragg´s diffraction angle. From the diffraction peak at $2\theta = 27.52°$ with $\beta = 0.0021$ rad and using the emission wavelength of the X-ray source (Cu-Kα, 1.5406 Å), an average crystal size of 68 nm can be calculated.

S2. Diffuse Reflectance Spectra of The Cr(VI)-TiO_2 Complex Formed Using Different TiO_2 Samples

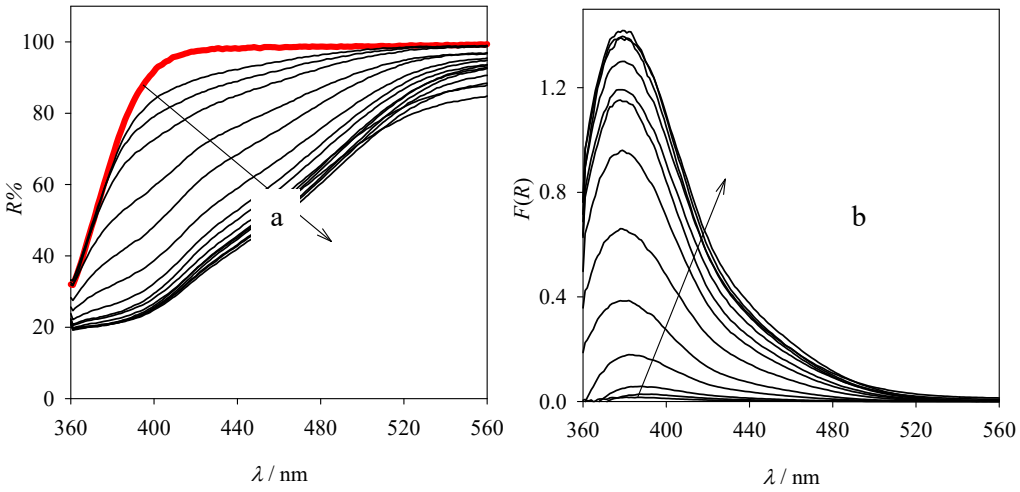

Figure S2. (**a**) Diffuse reflectance spectra of pure UV100 (thick red line) and UV100 after adsorption equilibrium with solutions containing Cr(VI) ($[Cr(VI)]_0$ = 2.5, 5, 10, 25, 50, 100, 175, 250, 375, 500, 675 and 750 µM, and 1, 1.25 and 1.5 mM, thin black lines); (**b**) remission function spectra of the same samples after subtraction of the remission function of pure UV100. Cr(VI) concentrations increase in the direction of the arrows.

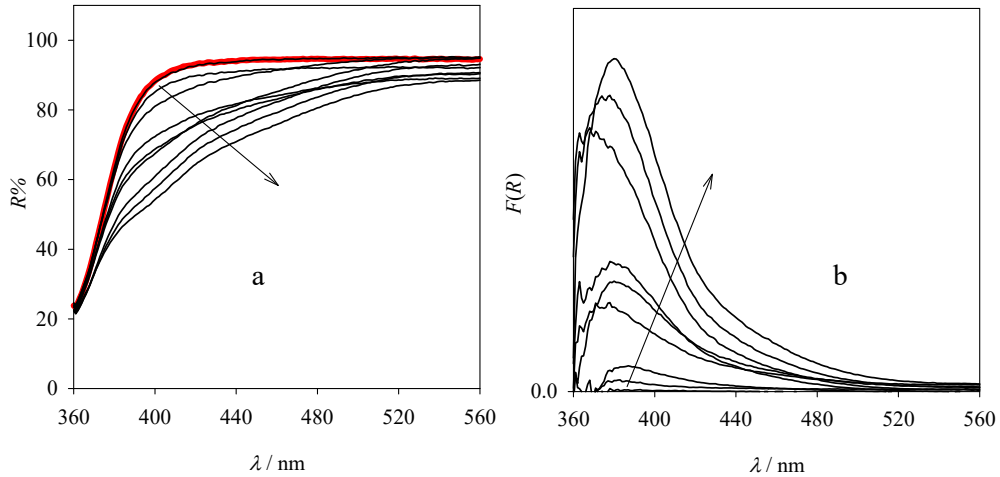

Figure S3. (a) Diffuse reflectance spectra of pure PC50 (thick red line) and PC50 after adsorption equilibrium with solutions containing Cr(VI) ($[Cr(VI)]_0$ = 5, 10, 25, 50, 100, 175, 250, 375, and 750 µM, thin black lines); (b) remission function spectra of the same samples after subtraction of the remission function of pure PC50. Cr(VI) concentrations increase in the direction of the arrows.

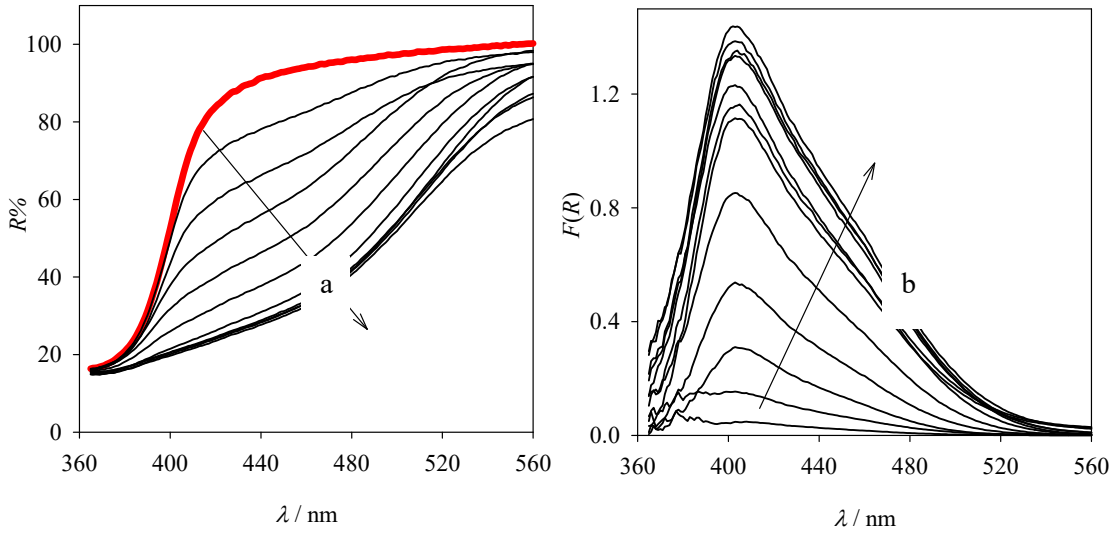

Figure S4. (a) Diffuse reflectance spectra of pure rutile sample (thick red line) and rutile sample after adsorption equilibrium with solutions containing Cr(VI) ($[Cr(VI)]_0$ = 5, 10, 25, 50, 100, 175, 250, 500, 625 and 750 μM, thin black lines); (**b**) remission function spectra of the same samples after subtraction of the remission function of pure rutile support. Cr(VI) concentrations increase in the direction of the arrows.

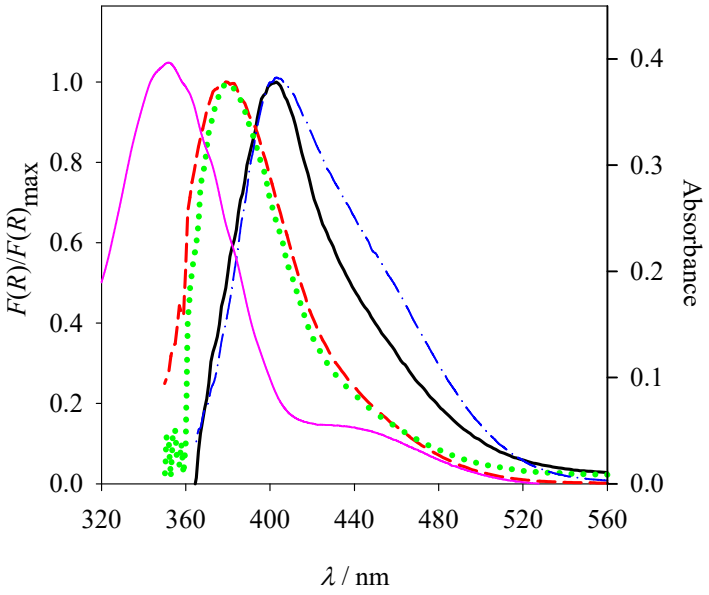

Figure S5. Normalized remission function spectra of Cr(VI) adsorbed on P25 (solid black line), UV100 (dashed red line), PC50 (dotted green line) and rutile (dash-dotted blue line) supports, compared with the absorption spectrum of 250 μM Cr(VI) (solid pink line) in aqueous solution at pH 2 ($HClO_4$).

S3. Equations Used for Multiple Gaussian Fittings

In order to compare absorption shapes and peaks positions of adsorbed Cr(VI) species (Cr(VI)-TiO_2 complex), normalized remission function spectra were analyzed by multiple Gaussian fittings considering Gaussian absorption bands (in wavelength scale) using the following equations: [1]

$$f(\lambda) = \sum_{i=1}^{n} a_i \times exp\left[\frac{-(\lambda - b_i)^2}{2 \times {c_i}^2}\right] \quad \text{(S2)}$$

$$\text{FWHM} = 2\sqrt{2 \times \ln 2} \times \sigma_i \quad \text{(S3)}$$

where a_i is the height of the corresponding Gaussian component, b_i is the position of its peak center (in nm), and σ_i represents the standard deviation of the function, related with the full width at half maximum (FWHM) of the component band (Equation (S3)).

In all cases, the best fits were achieved by considering two (n = 2) or three (n = 3) Gaussians. Fitting parameters for spectra of initial Cr(VI) concentrations above 250 μM are listed in Table S1 ($R^2 > 0.99$ was obtained in all cases). Spectra at lower initial concentrations were also analyzed leading to similar results but showing somewhat higher uncertainties due to experimental error. Similar fitting qualities were achieved by multiple Gaussian decomposition in energy scale (*e.g.*, for UV100: 3.39 ± 0.01 eV (366 nm, 14%), 3.23 ± 0.01 eV (385 nm, 56%), 2.95 ± 0.07 eV (420 nm, 30%)).

The present model considers that the absorption spectra of Cr(VI)-TiO_2 results from different Franck-Condon transitions from the same species or different Cr(VI) adsorbed species with Gaussian-type inhomogeneous broadening of the ensemble bands arising from different interactions within a heterogeneous environment [2,3]. Other models considering symmetric [1,4] or asymmetric Gaussians [5], Lorentz or mixed Gaussian-Lorentz (Voigt) curves in wavelength or energy scales might be considered [6], but the excellent fittings found here constitutes a first approach for spectral shape comparisons.

Table S1. Multiple Gaussian fitting parameters for initial Cr(VI) concentrations above 250 μM. The percentage areas were calculated related to the total area given by the sum of all components. All the band parameters were left free in these fits, assuming Gaussian bands on wavelength scale.

P25 (6 spectra)				
Comp.	*a*	*b* / nm	*FWHM* / nm	% area
G1	0.69 ± 0.07	397 ± 1	44 ± 2	41
G2	0.41 ± 0.03	430 ± 6	85 ± 9	48
G3	0.05 ± 0.02	506 ± 11	170 ± 30	11
Rutile (6 spectra)				
Comp.	*a*	*b* / nm	*FWHM* / nm	% area
G1	0.57 ± 0.07	401 ± 1	37 ± 1	27
G2	0.62 ± 0.04	435 ± 4	91 ± 4	73
UV100 (8 spectra)				
Comp.	*a*	*b* / nm	*FWHM* / nm	% area
G1	0.24 ± 0.02	370 ± 1	23 ± 1	8
G2	0.62 ± 0.03	385 ± 6	45 ± 1	42
G3	0.32 ± 0.02	406 ± 4	103 ± 6	50
PC50 (4 spectra)				
Comp.	*a*	*b* / nm	*FWHM* / nm	% area
G1	0.36 ± 0.11	366 ± 2	15 ± 5	10
G2	0.83 ± 0.11	379 ± 5	44 ± 4	66
G3	0.20 ± 0.02	408 ± 3	68 ± 8	24

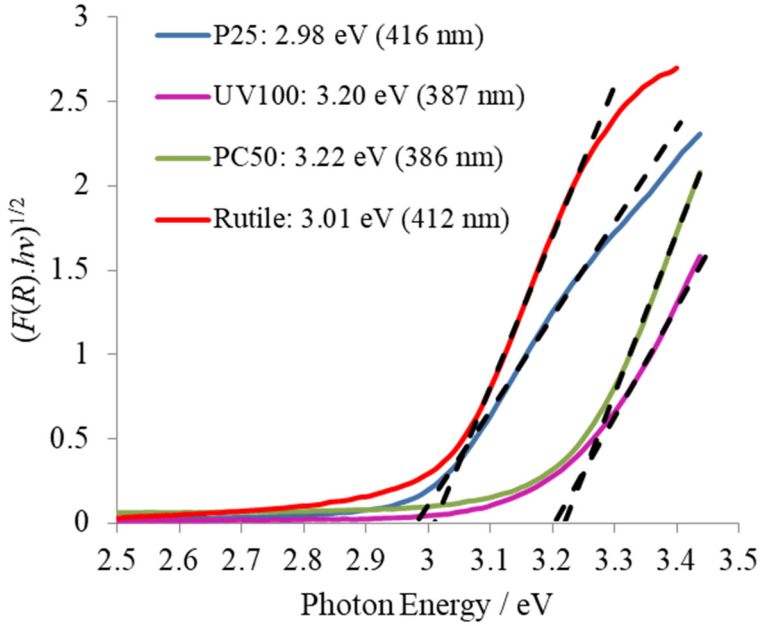

Figure S6. Tauc plots obtained from diffuse reflectance spectra and calculated optical band-gaps (± 0.02 eV) for the naked supports [7].

S4. Discussion about The Cr(VI)-TiO_2 Absorption Spectra

The results of Table S1 indicate that the absorption spectra of the Cr(VI)-TiO_2 complexes can be deconvoluted into two or three components, with the two main components of the rutile-containing samples (rutile and P25) ≈ 20 nm red-shifted compared to the anatase ones (PC50 and UV100), similar to the difference between the absorption onset of these TiO_2 crystalline structures. The anatase contribution of P25 can be masked by the rutile absorption. For all samples, the short-wavelength Gaussian main component peaks close to the optical band-gap wavelength of the naked semiconductors (see Figure S6). A direct photosensitization mechanism based on optical electron transfer (OET) from the valence band of TiO_2 to chemisorbed Cr(VI) species (*e.g.*, optically-allowed band-to-molecule charge transfer, VB $\rightarrow Cr^{VI}$) can be proposed, in agreement with similar systems where a strong electronic coupling of chemisorbed species is observed [8]. The OET mechanism is in line with the apparent correlation between the short-wavelength Gaussian main absorption component and the optical band-gap of the support. A band alignment of anatase and rutile TiO_2 placed the VB of rutile above (0.39 - 0.47 eV) the VB of anatase [9], thus predicting a red-shifted VB $\rightarrow Cr^{VI}$ absorption band for the rutile-Cr(VI) complexes compared with the anatase-Cr(VI) complexes, with shifts in the order of the optical band-gap differences of the naked supports (~0.2 eV, see Figure S6). However, Kuncewicz *et al.* [10] suggested that a ligand-to-metal ($O^{-II} \rightarrow Cr^{VI}$) charge transfer excitation of adsorbed chromate(VI) species on TiO_2 (broad UV-visible LMCT absorption band) leads to a Cr^{V}-O^{-I} excited species, followed by hole transfer from the excited Cr(VI) species to the VB (VB $\rightarrow O^{-I}$) that prevents, to some extent, $Cr^{V} \rightarrow O^{-I}$ charge recombination. Investigating whether this apparent correlation reflects the direct excitation of charge-transfer states between the adsorbed Cr(VI) and TiO_2 energy bands, or if results from the absorption of Cr(VI)-TiO_2 complex masked by the intense support absorption above its band-gap, requires thorough quantum-chemical calculations, which are out of the scope of the present work. Nevertheless, results point to the occurrence of a strong interaction between Cr(VI) and the surface of the catalysts, most probably in the form of a CT complex.

S5. Cr(VI) Adsorption Equilibria over The Different TiO_2 Samples

Adsorption isotherms calculated from mass balance of Cr(VI) in solution (Δ[Cr(VI)]) and from the concentration of the Cr(VI)-TiO_2 complex measured by diffuse reflectance are compared in Figure S7.

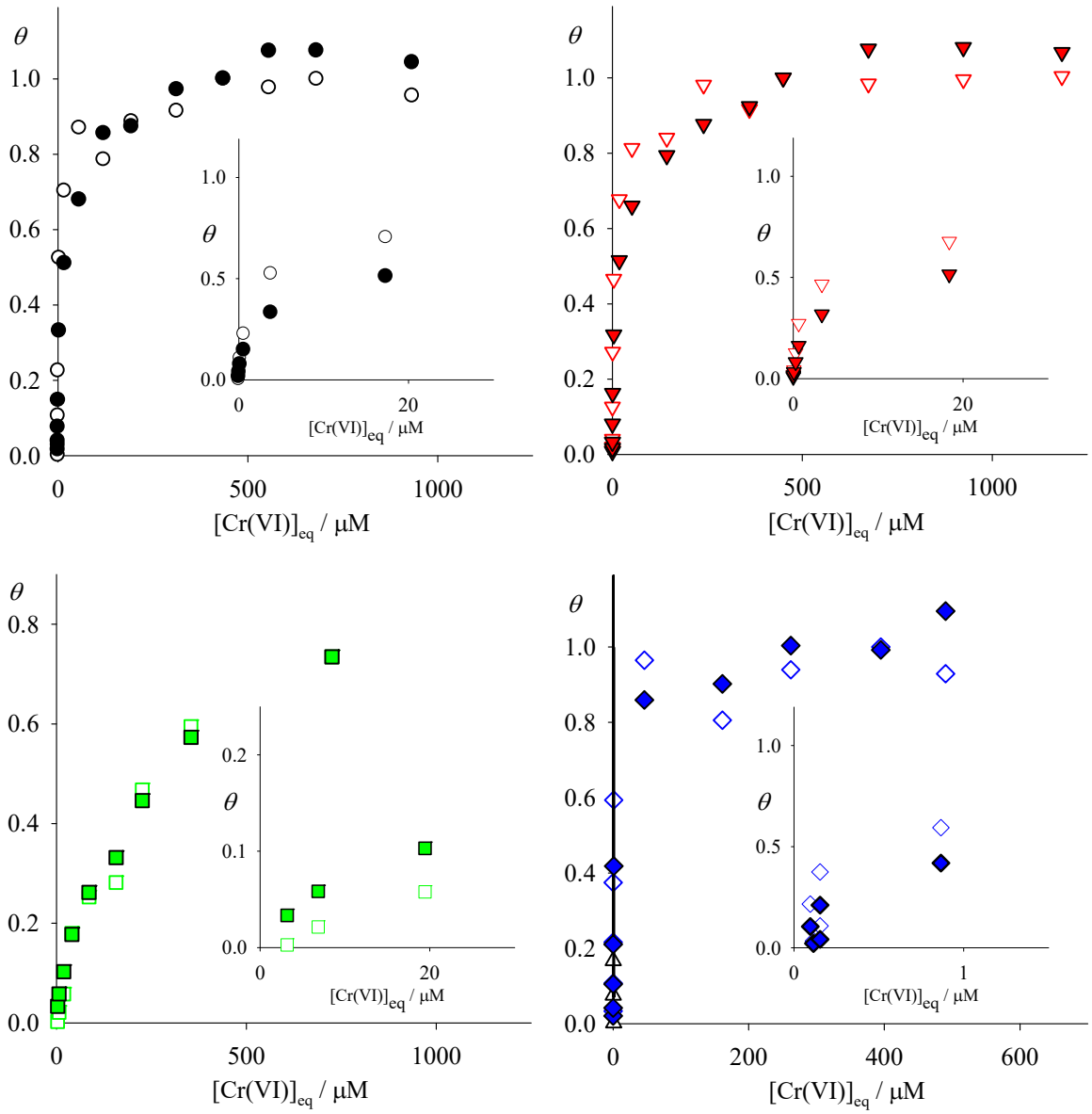

Figure S7. Compared calculated saturation degrees (θ) of Cr(VI) adsorption equilibrium on (**a**) P25, (**b**) UV100, (**c**) PC50, and (**d**) rutile, calculated from the difference between the concentrations of the initial and the equilibrated solutions ($\Delta[Cr(VI)]/\Delta[Cr(VI)]_{sat}$, filled symbols) and from the remission functions of the dry solids ($F(R)/F(R)_{max}$, open symbols). Inset: same data in the 0-20 µM range for P25, UV100 and PC50, and 0-1.5 µM range for rutile.

S6. Comparison between The Pseudo First-Order and The Mixed Zero- + First-Order Models for The Photocatalytic Reduction of Cr(VI) over The Different TiO_2 Samples

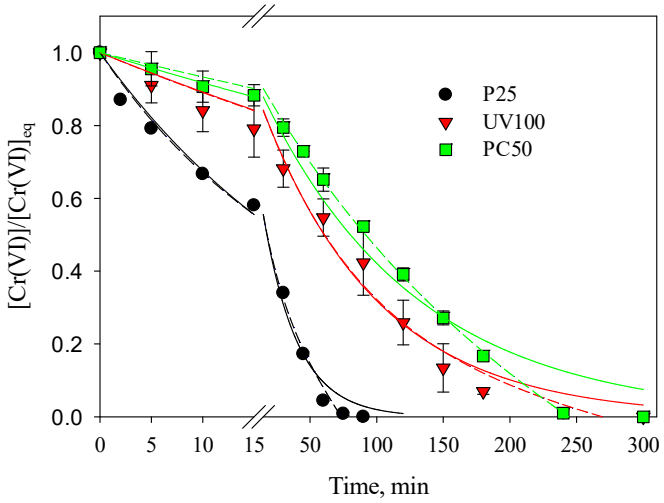

Figure S8. Temporal profile of normalized Cr(VI) concentration for the photocatalytic reduction over P25, UV100 and PC50. Initial conditions: $[Cr(VI)]_0$ = 0.8 mM, pH 2. Photon flux per unit volume incident on the wall of the cell ($q^0_{n,p}/V$): 7.8 μeinstein s^{-1} L^{-1}. Full lines are pseudo first-order fittings (Equation (S4)), dashed lines are mixed zero- + first-order fittings (Equation (S5)).

As can be appreciated, Cr(VI) decays are roughly first order (Equation (S4)), although a contribution from zero order is noticed in all cases (Equation (S5)).

$$\frac{[Cr(VI)]}{[Cr(VI)]_{eq,0}} = e^{-k_{Cr(VI)} \times t} \quad (S4)$$

$$\frac{[Cr(VI)]}{[Cr(VI)]_{eq,0}} = A \times e^{-k'_{Cr(VI)} \times t} + B - k_0 \times t \quad (S5)$$

In Equations (S4) and (S5), $[Cr(VI)]_{eq,0}$ is the Cr(VI) concentration in the aqueous phase after the equilibrium concentration was reached, $k_{Cr(VI)}$ and $k'_{Cr(VI)}$ are pseudo first-order kinetic constants, k_0 is the zero order kinetic constant, and A and B represent the fractional contribution of the first and zero-order processes, respectively, to the Cr(VI) reduction. Cr(VI) evolution in Figure 4 indicates that the contribution of the pseudo first-order process is more significant at initial times, while at longer times the zero-order process becomes dominant. This kinetic model has been observed previously for Cr(VI) photocatalytic reduction on supported TiO_2 [11]. This behavior is opposite to the Langmuir-Hinshelwood model, where initially the reaction rate is almost zero order as it is independent of concentration in solution; only when the product of the adsorption constant K_L and the bulk concentration of the studied pollutant is below 1, the reaction behaves as first order. The fitting parameters of the results of Figure S8 to Equations (S4) and (S5) are shown in Table S2.

Table S2. Fitting parameters of Equations (S4) and (S5) taken from Figure S8.

Equation (S4)		$k_{Cr(VI)} \times 10^3$ **(min^{-1})**			R^2
P25		39 ± 2			0.991
UV100		11 ± 1			0.984
PC50		8.6 ± 0.6			0.977
Equation (S5)	$k'_{Cr(VI)} \times 10^3$ **(min^{-1})**	$k_0 \times 10^3$ **(min^{-1})**	A	B	R^2
P25	58 ± 8	5 ± 1	0.63 ± 0.03	0.37 ± 0.02	0.993
UV100	13 ± 3	0.8 ± 0.3	0.82 ± 0.03	0.18 ± 0.07	0.985
PC50	8.4 ± 0.9	1.2 ± 0.1	0.74 ± 0.02	0.26 ± 0.02	0.993

Data of Table S2 indicate that, for the three photocatalyst, the pseudo first-order process is the more significant contributor to Cr(VI) removal. Only for PC50, a significant increase in R^2 was obtained when using Equation (S5), which has four fitting parameters, instead of the simpler (only one parameter) Equation (S4). For P25, the value of $k'_{Cr(VI)}$ obtained with Equation (S5) is higher than $k_{Cr(VI)}$ obtained with Equation (S4), but when pondered with the A parameter ($k_{Cr(VI)} \times A$), the obtained value is almost the same. P25 shows the higher kinetic constants for both zero- and first-order processes, reflecting the higher photocatalytic activity of this sample, while for UV100 the pseudo first-order process is more significant than for PC50.

References

1. Sunshine JM, Pieters CM, Pratt SF. Deconvolution of mineral absorption bands: An improved approach. *J. Geophys. Res.* **1990**, *10*, 6955–6966. doi: 10.1029/JB095iB05p06955
2. Zuehlsdorff TJ, Isborn CM. Modeling absorption spectra of molecules in solution. *Int. J. Quantum Chem.* **2019**, *119*, e25719. doi: 10.1002/qua.25719
3. Li C-W, Benjamin MM, Korshin GV. Characterization of NOM and its adsorption by iron oxide coated sand (IOCS) using UV and fluorescence spectroscopy. *J. Environ. Eng. Sci.* **2006**, *5*, 467–472. doi: 10.1139/s06-012
4. Yan M, Dryer D, Korshin GV, Benedetti MF. In situ study of binding of copper by fulvic acid: Comparison of differential absorbance data and model predictions. *Water Res.* **2013**, *47*, 588–596. doi: 10.1016/j.watres.2012.10.020
5. Zucchelli G, Jennings RC, Garlaschi FM. The presence of long-wavelength chlorophyll a spectral forms in the light-harvesting chlorophyll a/b protein complex II. *J. Photochem. Photobiol. B* **1990**, *6*, 381–394. doi: 10.1016/1011-1344(90)85112-A
6. Brown AJ. Spectral curve fitting for automatic hyperspectral data analysis. *IEEE Trans. Geosci. Remote Sens.* **2006**, *44*, 1601–1608. doi: 10.1109/TGRS.2006.870435
7. Makuła P, Pacia M, Macyk W. How To Correctly Determine the Band Gap Energy of Modified Semiconductor Photocatalysts Based on UV−Vis Spectra. *J. Phys. Chem. Lett.* **2018**, *9*, 6814–6817. doi: 10.1021/acs.jpclett.8b02892
8. Macyk W, Szaciłowski K, Stochel G, Buchalska M, Kuncewicz J, Labuz P. Titanium(IV) complexes as direct TiO_2 photosensitizers. *Coordination Chem. Rev.* **2010**, *254*, 2687–2701. doi: 10.1016/j.ccr.2009.12.037
9. D. O. Scanlon, C. W. Dunnill, J. Buckeridge, S. A. Shevlin, A. J. Logsdail, S. M. Woodley, C. R. A. Catlow, M. J. Powell, R. G. Palgrave, I. P. Parkin, G. W. Watson, T.W. Keal, P. Sherwood, A. Walsh, A. A.Sokol. Band alignment of rutile and anatase TiO_2. *Nature Mater.* 2013*, 12*, 798–801. doi: 10.1038/nmat3697
10. Kuncewicz J, Ząbek P, Kruczała K, Szaciłowski K, Macyk W. Photocatalysis Involving a Visible Light-Induced Hole Injection in a Chromate(VI)−TiO_2 System. *J. Phys. Chem. C* **2012**, *116*, 21762–21770. doi: 10.1021/jp3040715
11. Kleiman A, Vera ML, Meichtry JM, Litter MI, Márquez A. Photocatalytic experiments with TiO_2 coatings obtained by cathodic arc deposition. *Appl. Catal. B* **2011**, *101*, 676–681. doi: 10.1016/j.apcatb.2010.11.009